Available online at www.sciencedirect.com
ScienceDirect
Trans. Nonferrous Met. Soc. China 24(2014) 673−681
Transactions of Nonferrous Metals Society of China
www.tnmsc.cn

Anomalous yield and intermediate temperature brittleness behaviors of directionally solidified nickel-based superalloy

Li-yuan SHENG[1], Fang YANG[2], Jian-ting GUO[3], Ting-fei XI[1]

1. Shenzhen Institute, Peking University, Shenzhen 518057, China;
2. Shenzhen Airlines, Shenzhen Bao'an International Airport, Shenzhen 518128, China;
3. Institute of Metal Research, Chinese Academy of Sciences, Shenyang 110016, China

Received 10 April 2013; accepted 8 May 2013

Abstract: A nickel-based superalloy with good corrosion resistance was fabricated by directional solidification, and its microstructure and tensile properties at elevated temperatures were investigated. Microstructure observations reveal that the γ' precipitates are arrayed in the γ matrix regularly with some MC, Ni_5Hf and M_3B_2 particles distributed along the grain boundary. The tensile tests exhibit that the tensile properties depend on temperature significantly and demonstrate obvious anomalous yield and intermediate-temperature brittleness (ITB) behavior. Below 650 °C, the yield strength decreases slightly but the ultimate tensile strength almost has no change. When the temperature is between 650 °C and 750 °C, the yield and ultimate tensile strengths rise rapidly, and after then they both decrease gradually with temperature increasing further. The elongation has its minimum value at about 700 °C. The TEM examination exhibits that sharing of the γ' by dislocation is almost the main deformation mechanism at low temperatures, but the γ' by-pass dominates the deformation at high temperatures. The transition temperature from shearing to by-pass should be around 800 °C. The anomalous yield and intermediate-temperature brittleness behaviors should be attributed to the high content of γ'. In addition, the carbides and eutectic structure also contribute some to the ITB behaviors of the alloy.
Key words: nickel-based superalloy; directional solidification; anomalous yield; intermediate-temperature brittleness; microstructure

1 Introduction

Nickel-based superalloys, which are strengthened by γ' precipitates and solution alloying elements, are widely used in high temperature environment, due to their excellent creep properties, fatigue strength and good corrosion resistance [1−4]. Recently, with the development of the land-base and aerospace gas turbine engines, the turbine inlet temperature rises year by year to obtain high thermal efficiency, which requires the superalloy to have better creep and corrosion resistance. In order to meet these requirements, more refractory elements are added to the superalloy, which is beneficial to the creep but harmful to the mechanical properties [5−7]. To the superalloy, though the high-temperature creep and fatigue behavior are very important, having a good plastic deformation capability is also very necessary.

Generally, it can be expected a better elongation with the increase of temperature. However, for the superalloy and some other alloys, sometimes they exhibit obvious anomalous yield behavior and intermediate-temperature brittleness (ITB) characteristic, which is harmful to the application of these materials. The phenomena of ITB and anomalous yield behaviors have been reported in the last century and till now many investigations have been carried out on them [8]. The former researches [9−11] show that some polycrystal superalloys have the ITB behavior. However, the reports on the behavior of the directionally solidified nickel-based superalloy are relative few.

The experimental directionally solidified nickel-based superalloy, which consists of γ matrix, γ' precipitates, carbides, and minor borides, is designed to use in high-performance industrial gas turbines [12]. To possess excellent hot-corrosion and high-temperature oxidation resistance, the alloy contains 13% Cr and 10% Co. In addition, more W, Mo, Ta and Hf are added to increase its creep properties. The benefit can be obtained

Foundation item: Projects (2012BAI18B05, 2012BAI18B01) supported by the Twelfth Five-Year National Science & Technology Support Program of China; Project (2009CB93004) supported by the National Basic Researh Program of China
Corresponding author: Li-yuan SHENG; Tel: +86-18665806226; Fax: +86-755-26984814; E-mail: lysheng@yeah.net
DOI: 10.1016/S1003-6326(14)63110-1

from the combination of refractory elements; however, they also would influence the mechanical properties of the alloy inevitably. Therefore, in the present work, the study on the microstructure and elevated temperature mechanical properties of the directionally solidified experimental alloy is carried out.

2 Experimental

The chemical composition of directionally solidified alloy used in the present study is listed in Table 1. The alloy was remelted in a VIM25F vacuum induction furnace and directionally solidified in ZGD2 vacuum induction furnace. The temperature gradient was 80 °C/cm and the withdrawal rate was 8 mm/min. The directionally solidified specimen was heat treated in a electric muffle furnace with the procedure of (1210 °C, 2 h AC)+(1080 °C, 2 h AC)+(850 °C, 24 h AC) (AC: air cooling). The standard specimens for tensile test with a diameter of 5 mm and a gage length of 25 mm were machined longitudinally from the heat-treated samples. The tensile tests were conducted on a Universal AG−250KNE test machine in air with initial strain rates of 5×10^{-5} to 1.04×10^{-4} s^{-1} at 25−1000 °C. The tensile specimens were induction heated and the temperature was measured using a thermocouples placed in the gauge length. The temperature gradient of the gauge length was not exceeded ±2 °C. Load and extension were recorded directly. The displacement rate was maintained at 0.5 mm/min up to rupture. At least three identical specimens were tested at each temperature.

Table 1 Chemical composition of directionally solidified alloy (mass fraction, %)

C	B	Cr	Co	W	Mo
0.024	0.012	12.53	9.81	5.46	1.21
Al	Ti	Ta	Hf	Ni	
3.76	2.28	4.65	0.32	Bal.	

Samples for microstructure observation were cut from the heat-treated and fracture specimens. The samples were fabricated by conventional method and electrochemically etched with an electrolyte consisting of 20 g $CuSO_4$+100 mL HCl+5 mL H_2PO_4+100 mL H_2O. The microstructure and fracture surface after the tensile tests were examined by an optical microscope (OM) and a scanning electron microscope (SEM) with an energy-dispersive X-ray spectroscope (EDS). The slices for transmission electron microscopy (TEM) observation were cut from the heat-treated sample and gauge part of the specimens deformed at different temperatures normal to the loading axis. The thickness of the slices was about 0.5 mm and polished to 50 μm. The polished slices were shaped into 3 mm in diameter followed by ion milling to perforation. The TEM observation was carried out by a JEM−2010 operated at 200 kV.

3 Results and discussion

3.1 Microstructure of heat-treated alloy

The typical optical metallographic microstructures of the directionally solidified alloy are shown in Figs. 1(a) and (b). The dendrites in metallographic samples cut perpendicular to the solidification direction appear as bright cross. The precipitates and γ/γ' eutectic mainly distribute in the interdendritic region. At such a withdrawal rate, the dendrite column almost parallels the direction of the solidification. Further observation on the alloy exhibits that some precipitates and chrysanthemum-like γ/γ' eutectic form along the boundary of matrix, as shown in Fig. 1(c). The EDS results reveal that they are carbide, boride and intermetallic compounds. The image of the γ' shows that the precipitates exhibit well cuboid morphology, as shown in Fig. 1(d). Moreover, there are some small γ' particles with small proportion distributing in the matrix among γ' particles.

TEM observation on the γ' precipitate exhibits that the γ' cuboids with an average edge length of 400 nm are produced after the heat treatment, as shown in Fig. 2(a). The secondary sphere γ' with scores of nanometers in diameter precipitates in the matrix. Further observation on the grain boundary and the eutectic region reveal that many precipitates exist in these regions, as shown in Fig. 2(b). Combining with the selected area electron diffraction (SAED) patterns, it can be determined that most of the particles in the alloy are MC type carbide. The EDS results reveal that they contain a lot of Ti and W element, as shown in Fig. 2(c), so the carbide can be described as (Ti, W)C. The TEM observation also exhibits small precipitates along the MC boundary. The SAED pattern reveals that the small precipitates have an orthorhombic crystal structure, and the EDS test exhibits that it has a lot of Cr element, as shown in Fig. 2(d). Due to the high content of B addition in the alloy, and based on the former studies [13,14], such precipitates should be M_3B_2 type boride. In addition, the TEM observation still finds some Hf-rich particles forming at the grain boundary, as shown in Figs. 2(e) and (f). Combining with the former researches [15,16] and the SAED pattern, the Hf-rich particle can be determined as Ni_5Hf phase, which has a cubic crystal structure with $a=b=c=0.68$ nm, and the space group of $F\bar{4}3m$.

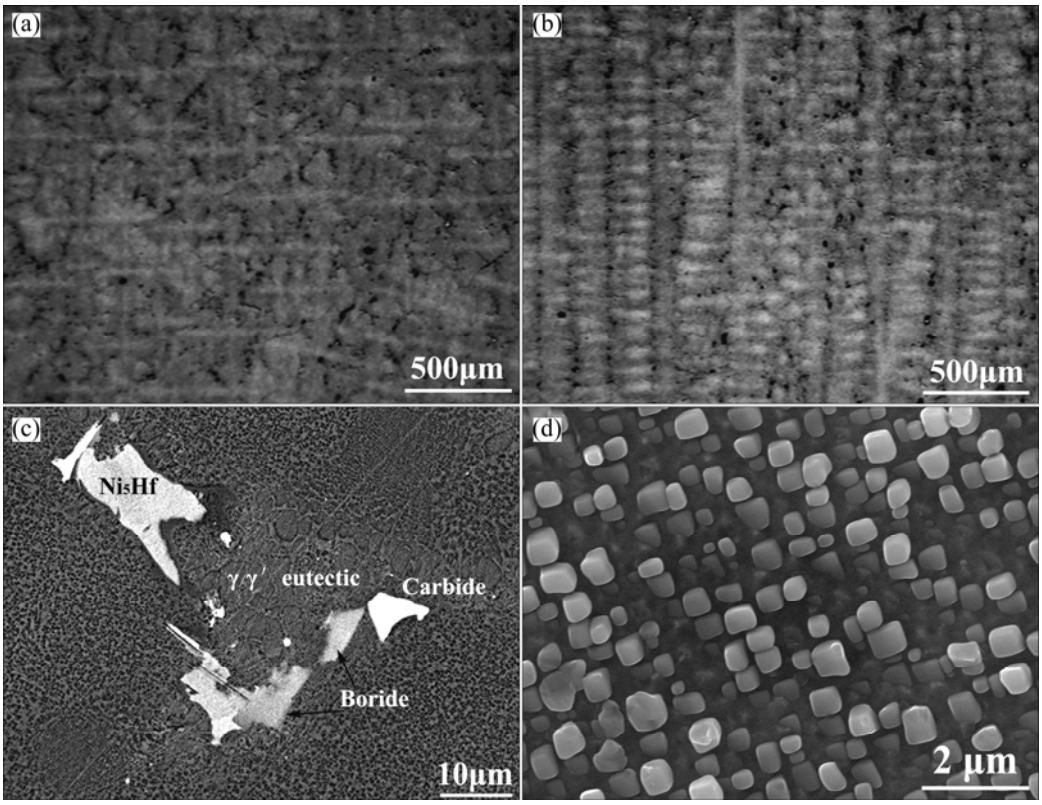

Fig. 1 OM micrographs of heat-treated directionally solidified alloy along transverse (a), longitudinal (b), SEM micrographs showing precipitates and γ/γ' eutectic (c) and cuboid γ' precipitates (d)

3.2 Mechanical properties

The tensile properties of the directionally solidified alloy at different temperatures are shown in Fig. 3. It can be seen that both yield strength and ultimate tensile strength decrease slightly with the increase of temperature. Then at about 650 °C the ultimate tensile strength and yield strength reach their minimum values. With further increase of temperature, ultimate tensile strength and yield strength increase again and obtain their maximum values at about 750 °C, and then they both drop rapidly. Different from changes of ultimate tensile strength and yield strength with temperature, reduction of area and elongation almost have no change below 600 °C, but they both decrease obviously and reach the minimum value at about 700 °C. The decrease of elongation is about 30%. Then reduction of area and elongation increase obviously. Comparing two figures, it can be found that there is a good correlation between the two trends, i.e. the increase of yield and ultimate tensile strengths corresponding to decrease in ductility in the same temperature range. Therefore, it can be concluded that the ITB behavior of the alloy is obvious.

It is well known that γ' has an interesting characteristic, namely its strength increases with temperature rising [17−19]. Due to the high volume fraction of γ' (about 60%) in the present alloy, the decrease in strength of the γ matrix with the increase of temperature is compensated by the increase of the strength from γ'. According to the former researches [17,20], the thermally activated cross-slip of dislocations from {111} planes to {110} planes would increase the strength of γ'. But beyond 900 °C, γ' dissolves rapidly, which induces the decrease of the alloy. In the present study, strength of the alloy changes little below 800 °C, but strength drops greatly when the temperature is higher.

According to Refs. [21,22], if the yield strength depends on the temperature greatly, the yielding behavior at elevated temperatures should possibly be a thermally activated process. Therefore, an Arrhenius type of relationship might be applicable to characterize the plastic flow behavior of this alloy, i.e.,

$$\sigma_y / E = A\{\exp[Q/(RT)]\} \quad (1)$$

where the σ_y is the yield strength, E is the elastic modulus, Q is the activation energy for the deformation process, T is the temperature, R is the gas constant, and A is a material constant. Equation (1) indicates that high-temperature strength is dominated by the dislocation−particle interaction, which has been studied by a large number of theoretical and experimental researches [9,23]. The plot of normalized value of yield strength

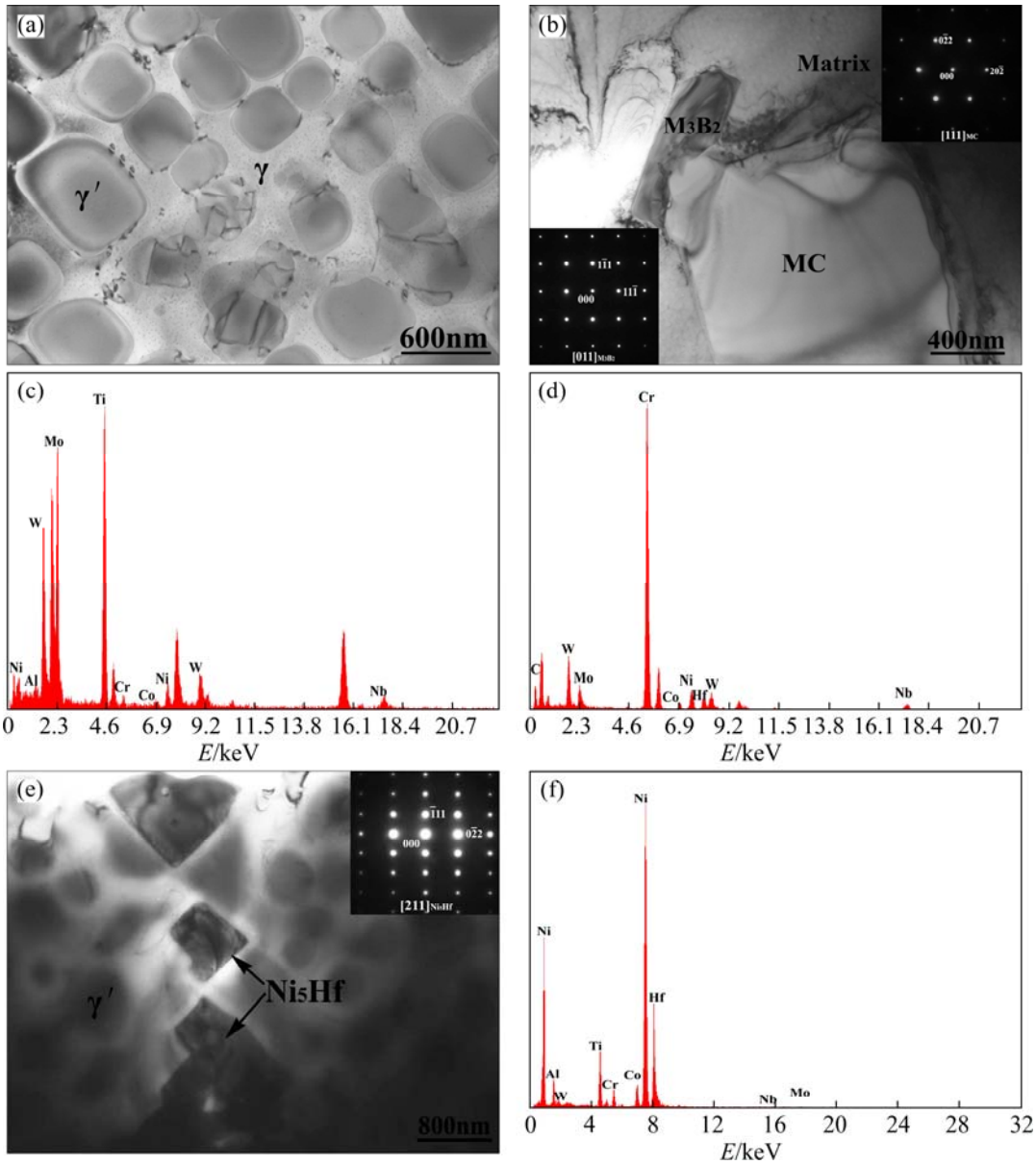

Fig. 2 Bright field TEM micrographs of γ′ precipitates (a), MC and M_3B_2 precipitates in interdendritic region (b), EDS results of MC (c) and M_3B_2 (d), TEM micrograph of Ni_5Hf particles along grain boundary (e) and EDS result of Ni_5Hf (f) (Insets show SAED patterns)

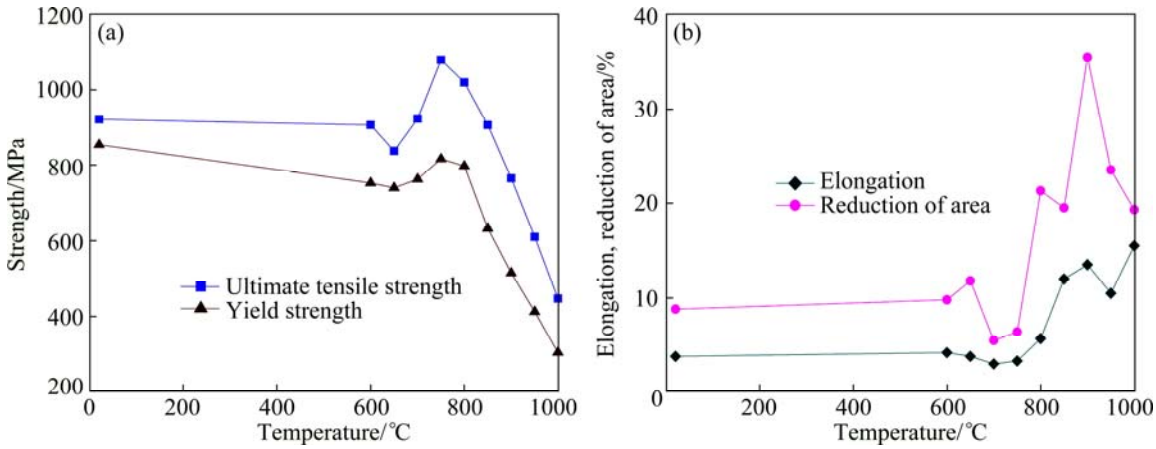

Fig. 3 Temperature dependence of ultimate tensile strength and yield strength (a), elongation and reduction of area (b)

by elastic modulus vs the inverse temperature is shown in Fig. 4. Clearly, there are three distinct temperature regimes. At high temperatures (above 750 °C), the curve has a positive slop, whereas at low temperatures (below 600 °C) and medium temperature, the curve exhibits a negative slop. This indicates a great change in the rate-controlling process for the deformation mechanism. The studied directionally solidified alloy is mainly strengthened by γ' precipitates which are the main obstacles for the dislocation moving. So, at low and medium temperatures, the high applied stress could force the dislocations to cut γ' particles. When the temperature increases, the applied stress is less than that required for dislocation cutting γ' precipitates, and then the role of thermal activation is strengthened, dislocation climb mechanism operates. So, one can see that the activation energy for deformation decreases obviously with temperature increasing.

The TEM observation on the alloy tested at different temperatures is shown in Fig. 5. Clearly, at room temperature, relative few dislocations are present and the spacing between dislocations is large. At 650 °C, the dislocation density becomes high, and the structure consists of less slip bands. Moreover, the dislocations tangle in the γ channel, which indicates that the matrix is still the main deformation region. When the temperature increases to 750 °C, it can be seen that dislocations with higher density form at γ'/γ interface and tangle with each other. Some dislocations pairs cut γ'particles and a number of stacking faults and microtwins are produced

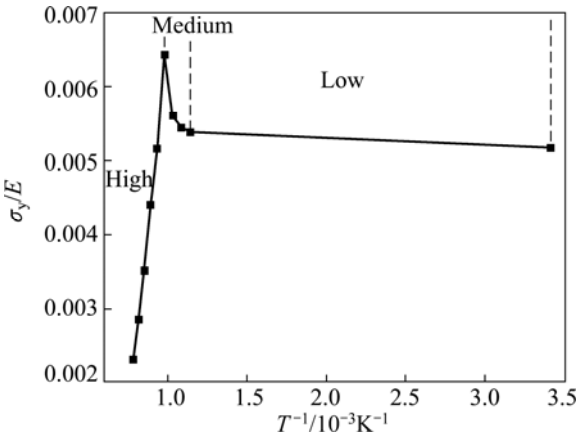

Fig. 4 Plot of σ_y/E vs inverse temperature

inside the γ', which indicates that the slipping system in the γ' is still difficult to start. Based on the recent study [11], the high yield strength of γ' is mainly due to the addition of elements, such as W and Ta. While in the present alloy, it contains a lot of W, Ta and Hf, so it is no doubt that it will increase the strength of the γ'. Therefore, it can be seen that the distribution of the dislocations in the alloy is nonhomogenous, which implies that the deformability at such a temperature is still bad. Differing from the sharing at low and intermediate temperatures, the deformation of the alloy at high temperatures is primarily dominated by dislocation moving around the γ' precipitates. The TEM micrograph of the alloy tested at 900 °C exhibits the typical dislocation structures that

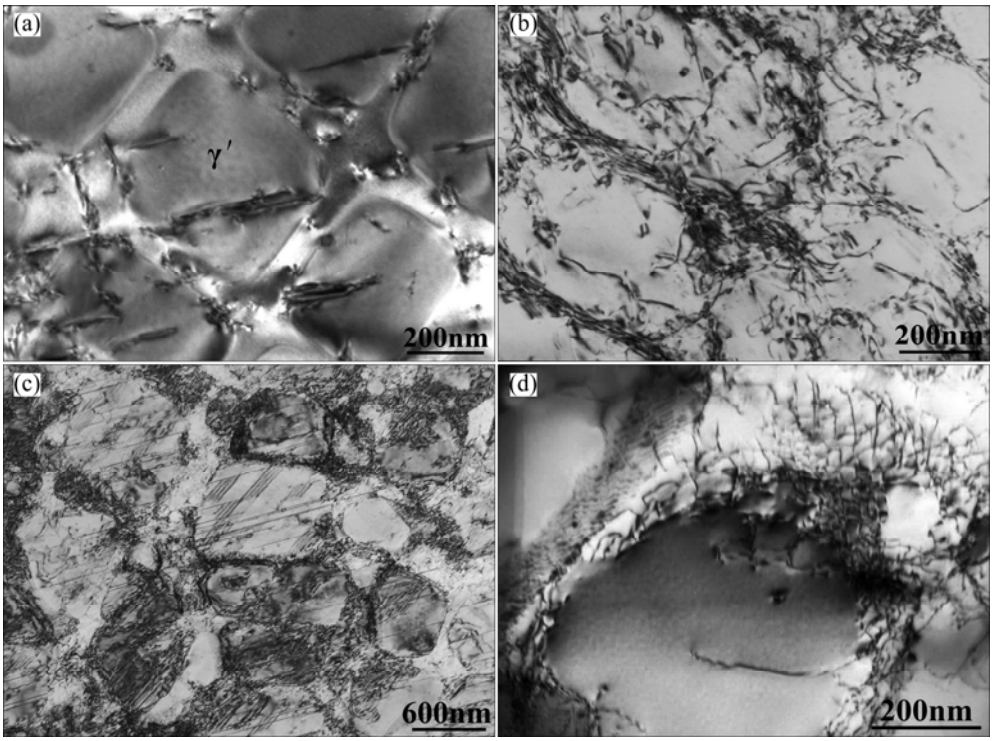

Fig. 5 Bright field TEM micrographs of tensile specimens tested at different temperatures: (a) Room temperature; (b) 650 °C; (c) 750 °C; (d) 900 °C

weave between the γ' particles and wrap around them. Dislocations are only infrequently observed within the γ', so the deformation is dominated by γ' by-pass at such a temperature. These observations confirm the calculated results in Fig. 4 that below 750 °C the thermal activation energy for the deformation increases greatly because of almost no climb dislocations in the alloy.

3.3 Fracture surface morphology

The morphologies of fracture surface of the tensile specimens tested at room temperature and 650 °C are shown in Fig. 6. Clearly, the quasi-cleavage and decohesion combined with some dimples are the main characteristics in the specimen tested at room temperature, as shown in Fig. 6(a). In general, the alloy exhibits semi-brittle features at room temperature, so it can be seen that the elongation and fracture shortage are so low at this condition. Though there are some dimples, the tear-off dimples were not elongated, so the deformation by the shear mode is limited. Facets develop in conjunction with decohesion region and appear as rounded surface morphology. When the tested temperature increases to 650 °C, it can be found that fractograph changes obviously, as shown in Fig. 6(b). The cleavage decreases but the dimple increases greatly. However, the elongation of the alloy almost has no change, compared with it at room temperature. Further observations reveal that many cracked MC carbides and decohesion along the carbide/matrix interface exist on the fracture surface. The cracks can propagate along the rigid precipitates and matrix easily, which is harmful to the ductility [24−27]. Therefore, it is easy to understand why the elongation of the alloy at 650 °C is still low.

The fracture surface of the alloy tested at 750 °C is shown in Figs. 7(a) and (b). It can be seen that it exhibits more brittle characteristics, and cleavage is the main feature, as shown in Fig. 7(a). Secondary cracks propagate along the grain boundary and distribute randomly. Moreover, small dimples and carbides distribute on the cleavage facets. Further observation also finds the flowery cleavage feature in some adjacent regions, as shown in Fig. 7(b). When the tested temperature increases to 800 °C, it can be found that the dimples increase and secondary crack decreases obviously, as shown in Fig. 7(c). However, at this temperature, the alloy still exhibits obvious brittle fracture characteristics, so cleavage is the main feature. While the fractograph of the alloy tested at 900 °C displays more ductile characteristic, and the dimples with different sizes are the main feature. Then it can be postulated that the γ' begins to soften, when the temperature exceeds 800 °C, so more dislocations are activated. Therefore, the deformation is more homogeneous, and plenty of dimples are observed on the fracture surface.

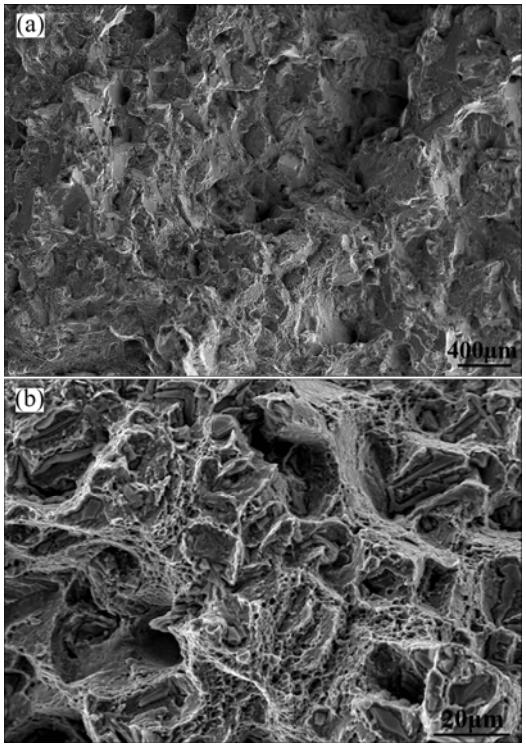

Fig. 6 SEM images of tensile specimen at room temperature showing semi-brittle features (a) and at 650 °C exhibiting combination of dimple and cleavage (b)

According to the recent studies on the unusual variation of tensile properties in superalloy at elevated temperatures [11,28], it can be concluded that the anomalous yield and the ITB behavior of the present alloy should mainly be attributed to the γ' precipitates. Due to its intrinsic characteristic, the strength of γ' increases with the temperature rising [29]. Therefore, the decrease of yield strength caused by the γ matrix at elevated temperatures could be compensated by γ', due to the high volume fraction of γ'. Then the yield strength and ultimate strength increase between 650 °C and 750 °C. Moreover, at the temperature below 750 °C, the γ matrix has already yielded, and the dislocations would accumulate along the γ', which strengthens the alloy further. However, it is still very difficult for the dislocation to cross the γ', and then the high accumulation of dislocations along the γ' would lead to the generation of crack. So, it can be found that many debondings along interface and secondary cracks exist in the specimen tested at 750 °C, and the elongation at this temperature is the lowest. In addition, the formation of superlattice-intrinsic stacking faults (S-ISFs) formed in the γ' contributes to the ITB behavior. Based on the previous researches [9,10], the formation of S-ISFs is beneficial to the strength but detrimental to the ductility.

While in the present alloy, the stacking faults form at 750 °C obviously, which will make the ITB phenomenon worse. When the temperature is higher than 750 °C, diffusion-controlling process becomes dominated, so more dislocations and slip system can be activated. The deformation becomes easier with the increase of temperature, and then the elongation increases gradually. Besides the γ', the carbides, grain boundary and eutectic structure also have influence on the ITB behavior. Due to the relative low solidification rate, the impurity and elements with big atom radius will be rejected to the grain boundary, which is harmful to the cohesion of the grain boundary. Once the stress concentrates along the grain boundary, it will result in the crack. And moreover, the relative low cohesion will promote the crack to propagate along the grain boundary, as shown in Fig. 8(a). Additionally, the bulk carbides and γ/γ' eutectic structure are also detrimental to the elongation. The relatively large size and high stiffness make it difficult for the dislocation to shear, which results in higher

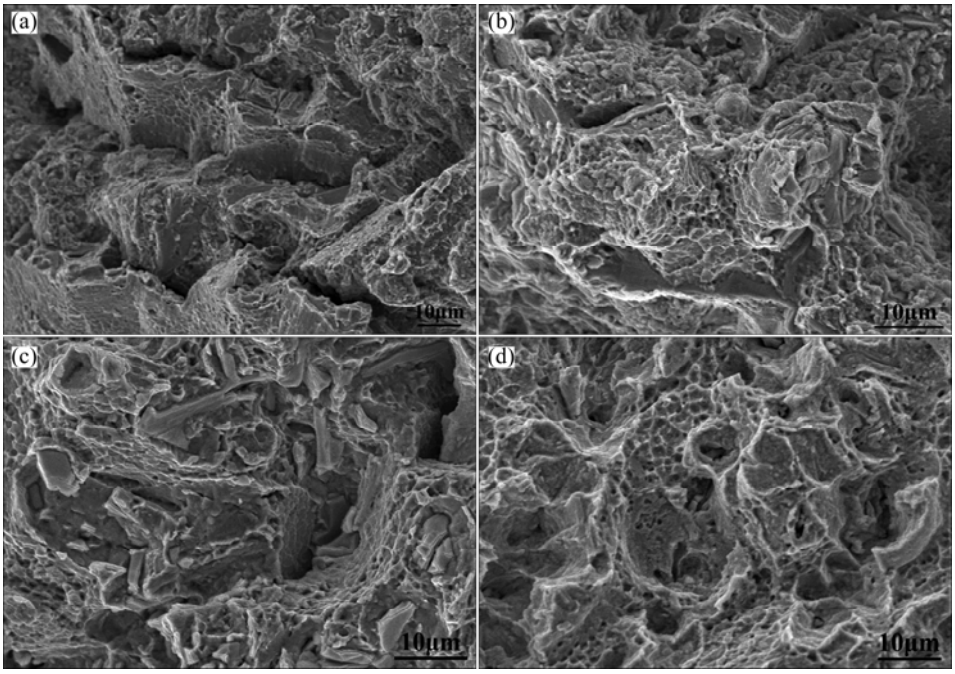

Fig. 7 Fracture surface of tensile specimen at 750 °C showing cleavage feature (a), small dimples on cleavage surface (b), combination of dimple and cleavage on fracture surface at 800 °C (c) and full dimples characteristic of tensile specimen at 900 °C (d)

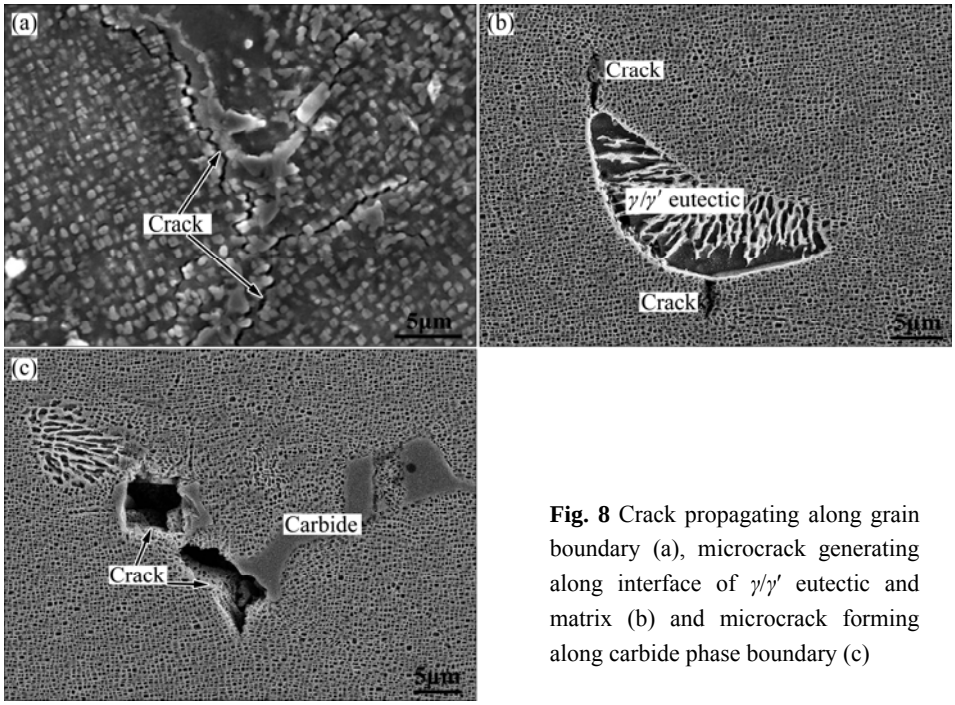

Fig. 8 Crack propagating along grain boundary (a), microcrack generating along interface of γ/γ' eutectic and matrix (b) and microcrack forming along carbide phase boundary (c)

concentration of stress along their interfaces. Then one can see that the crack is easy to generate along the interfaces of carbides and γ/γ' eutectic structure, as shown in Figs. 8(b) and (c).

4 Conclusions

1) The superalloy with high content of refractory elements is fabricated by directional solidification. Microstructure observations show that besides the γ' precipitates and γ matrix, some MC, Ni_5Hf and M_3B_2 particles precipitate along the grain boundary.

2) The tensile test reveals that the directionally solidified superalloys exhibit obvious anomalous yield and ITB behavior at medium temperatures and obtains its minimum elongation at about 700 °C.

3) The anomalous yield and ITB behavior of the directionally solidified superalloy should be mainly ascribed to the γ' precipitates. In addition, the carbides and eutectic structure also contribute to the ITB behaviors.

References

[1] REED P A S, SINCLAIR I, WU X D. Fatigue crack path prediction in UDIMET 720 nickel-based alloy single crystals [J]. Metallurgical and Materials Transactions A, 2000, 31: 109−123.

[2] SHENG L Y, YANG F, XI T F, LAI C, GUO J T. Microstructure and elevated temperature tensile behaviour of directionally solidified nickel based super alloy [J]. Materials Research Innovations, 2013, 17(s1): 101−106.

[3] SCZERZENE F, MAURER G E. Developments in disc materials [J]. Materials Science and Technology, 1987, 3(9): 733−742.

[4] SHENG Li-yuan, XI Ting-fei, LAI Chen, GUO Jian-ting, ZHENG Yu-feng. Effect of extrusion process on microstructure and mechanical properties of Ni_3Al−B−Cr alloy during self-propagation high-temperature synthesis [J]. Transactions of Nonferrous Metals Society of China, 2012, 22(3): 489−495.

[5] SHIMABAYASHI S, KAKEHI K. Effect of ruthenium on compressive creep of Ni-based single-crystal superalloy [J]. Scripta Materialia, 2010, 63(9): 909−912.

[6] SHENG L Y, XIE Y, XI T F, GUO J T, ZHENG Y F, YE H Q. Microstructure characteristics and compressive properties of NiAl-based multiphase alloy during heat treatments [J]. Materials Science and Engineering A, 2011, 528(29−30): 8324−8331.

[7] SHENG L Y, ZHANG W, GUO J T, ZHOU L Z, YE H Q. Microstructure evolution and mechanical properties' improvement of NiAl−Cr(Mo)−Hf eutectic alloy during suction casting and subsequent HIP treatment [J]. Intermetallics, 2009, 17(12): 1115−1119.

[8] FIORE N F. Mid-range ductility minimum in Ni-base superalloys [J]. Rev High Temp Mater, 1975, 2: 373−408.

[9] HE L Z, ZHENG Q, SUN X F, HOU G C, GUAN H R, HU Z Q. Low ductility at intermediate temperature of Ni-base superalloy M963 [J]. Materials Science and Engineering A, 2004, 380(1−2): 340−348.

[10] BETTGE D, OSTERLE W, ZIEBS J. Temperature dependence of yield strength and elongation of the Ni-base superalloy IN-738LC and the corresponding microstructural evaluation [J]. Z Metallkd, 1995, 86: 190−197.

[11] KIM I S, CHOI B G, HONG H U, YOO Y S, JO CY. Anomalous deformation behavior and twin formation of Ni-base superalloys at the intermediate temperatures [J]. Materials Science and Engineering A, 2011, 528(24): 7149−7155.

[12] HOU J S, GUO J T, YANG G X, ZHOU L Z, QIN X Z, YE H Q. The microstructural instability of a hot corrosion resistant superalloy during long-term exposure [J]. Materials Science and Engineering A, 2008, 498(1−2): 349−358.

[13] VINCENT R. Precipitation around welds in the nickel-base superalloy Inconel 718 [J]. Acta Metallurgica, 1985, 33(7): 1205−1216.

[14] SHULGA A V. Boron and carbon behavior in the cast Ni-base superalloy EP962 [J]. Journal of Alloys and Compounds, 2007, 436(1−2): 155−160.

[15] SHENG Li-yuan, YANG Fang, XI Ting-fei, ZHENG Yu-feng, GUO Jian-ting. Microstructure and room temperature mechanical properties of NiAl–Cr(Mo)–(Hf, Dy) hypoeutectic alloy prepared by injection casting [J]. Transactions of Nonferrous Metals Society of China, 2013, 23(4): 983−990.

[16] SHENG L Y, YANG F, XI T F, ZHENG Y F, GUO J T. Improvement of compressive strength and ductility in NiAl–Cr(Nb)/Dy alloy by rapid solidification and HIP treatment [J]. Intermetallics, 2012, 27: 14−20.

[17] STOLOFF N S. Physical and mechanical metallurgy of Ni_3Al and its alloys [J]. International Materials Reviews, 1989, 34: 153−183.

[18] SHENG L Y, ZHANG W, GUO J T, WANG Z S, OVCHARENKO V E, ZHOU L Z, YE H Q. Microstructure and mechanical properties of Ni_3Al fabricated by thermal explosion and hot extrusion [J]. Intermetallics, 2009, 17(7): 572−577.

[19] SHENG L Y, YANG F, XI T F, GUO J T, YE H Q. Microstructure evolution and mechanical properties of Ni_3Al/Al_2O_3 composite during self-propagation high-temperature synthesis and hot extrusion [J]. Materials Science and Engineering A, 2012, 555: 131−138.

[20] KOLBE M, NEUKING K, EGGELER G. Dislocation reactions and microstructural instability during 1025 °C shear creep testing of superalloy single crystals [J]. Materials Science and Engineering A, 1997, 234−236: 877−879.

[21] SENGUPTA A, PUTATUNDA S K, BARTOSIEWICZ L, HANGAS J, NAILOS P J, PEPUTAPECK M, ALBERTS F E. Tensile behavior of a new single crystal nickel-based superalloy (CMSX-4) at room and elevated temperatures [J]. Journal of Materials Engineering and Performance, 1994, 3(1): 664−672.

[22] PU Z J, WU K H, SHI J, ZOU D. Development of constitutive relationships for the hot deformation of boron microalloying TiAlCrV alloys [J]. Materials Science and Engineering A, 1995, 192−193: 780−787.

[23] MCLEAN M. On the threshold stress for dislocation creep in particle strengthened alloys [J]. Acta Metallurgica, 1985, 33(4): 545−556.

[24] SHENG L Y, YANG F, GUO J T, XI T F, YE H Q. Investigation on NiAl−TiC−Al_2O_3 composite prepared by self-propagation high temperature synthesis with hot extrusion [J]. Composites Part B: Engineering, 2013, 45(1): 785−791.

[25] SHENG L Y, YANG F, XI T F, GUO J T. Investigation on microstructure and wear behavior of the NiAl−TiC−Al_2O_3 composite fabricated by self-propagation high-temperature synthesis with extrusion [J]. Journal of Alloys and Compounds, 2013, 554: 182−188.

[26] SHENG L Y, GUO J T, REN W L, ZHANG Z X, REN Z M, YE H Q. Preliminary investigation on strong magnetic field treated NiAl–Cr(Mo)–Hf near eutectic alloy [J]. Intermetallics, 2011, 19(2): 143−148.

[27] SHENG L Y, ZHANG W, GUO J T, WANG Z S, YE H Q. Microstructure evolution and elevated temperature compressive properties of a rapidly solidified NiAl–Cr(Nb)/Dy alloy [J]. Materials

and Design, 2009, 30(7): 2752−2755.
[28] CHU Z K, YU J J, SUN X F, GUAN H R, HU Z Q. Tensile property and deformation behavior of a directionally solidified Ni-base superalloy [J]. Materials Science and Engineering A, 2010, 527(12): 3010−3014.
[29] CAILLARD D, PAIDAR V. A model for the anomalous mechanical properties of nickel-base L_{12} ordered alloys-I. Dislocations dynamics [J]. Acta Materialia, 1996, 44(7): 2759−2771.

定向凝固镍基高温合金的反常屈服和中温脆性行为

盛立远[1]，杨 芳[2]，郭建亭[3]，奚廷斐[1]

1. 北京大学 深圳研究院，深圳 518057；
2. 深圳宝安国际机场 深圳航空有限责任公司，深圳 518128；
3. 中国科学院 金属研究所，沈阳 110016

摘 要：采用真空冶炼和定向凝固工艺制备一种具有优异抗腐蚀性能的镍基高温合金，并利用光学显微镜、扫描电镜和透射电镜研究合金的微观组织，分析合金在不同温度下的拉伸性能。结果表明，除 γ′颗粒和 γ 基体外，在合金晶界上析出了一些 MC 碳化物、M_3B_2 硼化物和 Ni_5Hf 相。合金拉伸性能对温度有很强的依赖性，并呈现明显的的反常屈服和中温脆性行为。在 650 °C 以下，合金的屈服强度随着温度的升高而略微降低，但抗拉强度几乎没有变化。当温度在 650 °C 和 750 °C 之间时，合金的屈服、抗拉强度快速升高，但拉伸塑性显著降低，并在 700 °C 时达到最低值。当温度进一步升高时，合金的屈服、抗拉强度逐渐降低，塑性升高。透射电镜观察发现，在低温条件下，位错切割 γ′是主要的变形机制；在高温条件下，位错绕过 γ′是主要的变形机制；由位错切割 γ′转变至位错绕过 γ′的温度约为 800 °C。合金的反常屈服和中温脆性行为主要归因于合金中高的 γ′含量。此外，碳化物和共晶组织对合金的中温脆性行为也有影响。

关键词：镍基高温合金；定向凝固；反常屈服；中温脆性；微观组织

(Edited by Xiang-qun LI)